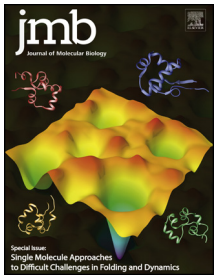

Ultrafast Protein Folding in Membrane-Mimetic Environments

Georg Krainer [1,2], Andreas Hartmann [1], Abhinaya Anandamurugan [1], Pablo Gracia [1], Sandro Keller [2] and Michael Schlierf [1]

*1 - **B CUBE—Center for Molecular Bioengineering,** Technische Universität Dresden, Arnoldstr. 18, 01307 Dresden, Germany*
*2 - **Molecular Biophysics,** University of Kaiserslautern, Erwin-Schrödinger-Str. 13, 67663 Kaiserslautern, Germany*

***Correspondence to Georg Krainer, Sandro Keller and Michael Schlierf:** G. Krainer and M. Schlierf are to be contacted at: B CUBE–Center for Molecular Bioengineering, Technische Universität Dresden, Arnoldstr. 18, 01307 Dresden, Germany; S. Keller is to be contacted at: Molecular Biophysics, University of Kaiserslautern, Erwin-Schrödinger-Str. 13, 67663 Kaiserslautern, Germany georg.krainer@tu-dresden.de; mail@sandrokeller.com; michael.schlierf@tu-dresden.de*
https://doi.org/10.1016/j.jmb.2017.10.031

Abstract

Proteins fold on timescales from hours to microseconds. In addition to protein size, sequence, and topology, the environment represents an equally important factor in determining folding speed. This is particularly relevant for proteins that require a lipid membrane or a membrane mimic to fold. However, only little is known about how properties of such a hydrophilic/hydrophobic interface modulate the folding landscape of membrane-interacting proteins. Here, we studied the influence of different membrane-mimetic micellar environments on the folding and unfolding kinetics of the helical-bundle protein Mistic. Devising a single-molecule fluorescence spectroscopy approach, we extracted folding and unfolding rates under equilibrium conditions and dissected the contributions from different detergent moieties to the free-energy landscape. While both polar and nonpolar moieties contribute to stability, they exert differential effects on the free-energy barrier: Hydrophobic burial stabilizes the folded state but not the transition state in reference to a purely aqueous environment; by contrast, zwitterionic headgroup moieties stabilize the folded state and, additionally, lower the free-energy barrier to accelerate the folding of Mistic to achieve ultrafast folding times down to 35 μs.

Introduction

Proteins fold into their native structures on timescales spanning at least six orders of magnitude [1], with some proteins exhibiting ultrafast folding times of $\tau_F < 100$ μs close to the protein-folding speed limit [2]. The principles determining folding speed are increasingly well understood, and many water-soluble proteins obey simple scaling laws [3,4]. For small two-state folders, which have to overcome one dominant free-energy barrier and whose folding is majorly driven by the hydrophobic effect, folding speed is primarily determined by peptide chain length [5], amino acid sequence [6], and topological complexity (e.g., contact order) [7,8]. However, an additional important—but often disregarded—factor in sculpting protein-folding kinetics is the protein's environment. Folding often takes place in surroundings that are far more multifaceted than bulk aqueous solutions, in which additional driving forces contribute to the folding process [9]. This is evident in cases such as folding under macromolecular crowding conditions or within cells [10–12]; yet, quantitative knowledge of the environmental modulation of other complex folding scenarios is still limited.

A particularly intricate folding situation that involves numerous molecular interactions is encountered for membrane-interacting proteins, which require the highly complex, anisotropic environment of a lipid-bilayer membrane or a membrane mimic to acquire their native folds [13,14]. The chemically and physically heterogeneous hydrophilic/hydrophobic interface

provided by such an environment features different properties and presents a multitude of polar and nonpolar contacts, such that changes in chemical composition can have a tremendous impact on the folding process [15–18]. This is particularly relevant for proteins that, for functional or evolutionary reasons, need to insert into or associate with membranes without relying on elaborate machineries like chaperones and translocons. In recent years, an increasing number of membrane proteins have become accessible to reversible unfolding/refolding studies from lipid-bilayer or membrane-mimetic systems, and several techniques adapted from water-soluble proteins have shed light on the molecular forces that control their folding [19–21]. However, only very little is known about how the properties of membrane mimics modulate their folding free-energy landscape; in particular, it remains unclear how largely divergent equilibrium stabilities are reflected in the kinetics of the folding and the unfolding reactions, as kinetic studies in the presence of membrane mimics are challenging for two principal reasons. First, classical two-state analysis of kinetic data obtained using lipid vesicles as membrane models is compounded by the fact that membrane insertion of a folding polypeptide chain is a complex, multi-step process that often involves accumulation of partially folded, membrane-adsorbed intermediates [22,23]. Second, micellar membrane mimics can alleviate these issues but are incompatible with conventional ensemble perturbation/relaxation techniques such as stopped-flow or temperature-jump experiments, as sudden environmental changes modulate the structural and dynamic properties of micelles [24], superimposing a second kinetic process that is hard if not impossible to separate out.

To overcome these limitations, several methods have been developed that allow access to kinetic information from measurements performed under equilibrium conditions. These include peak-shape analysis of nuclear magnetic resonance (NMR) spectra [25], statistical-thermodynamic treatment of protein-unfolding endotherms obtained by differential scanning calorimetry [26], and analysis of protein kinetics derived from single-molecule fluorescence experiments [27,28]. In particular, single-molecule Förster resonance energy transfer (FRET) spectroscopy, owing to its sensitivity and temporal resolution, is a powerful technique for disentangling intricate folding scenarios and extracting folding kinetics in membrane mimics from equilibrium measurements on timescales from hours down to microseconds, without the need of synchronization and complications arising from the superposition of micellar reorganization [28–31].

Here, we have devised an experimental system relying on single-molecule FRET spectroscopy that provides kinetic insights into the environmental modulation of a protein-folding reaction shaped by a

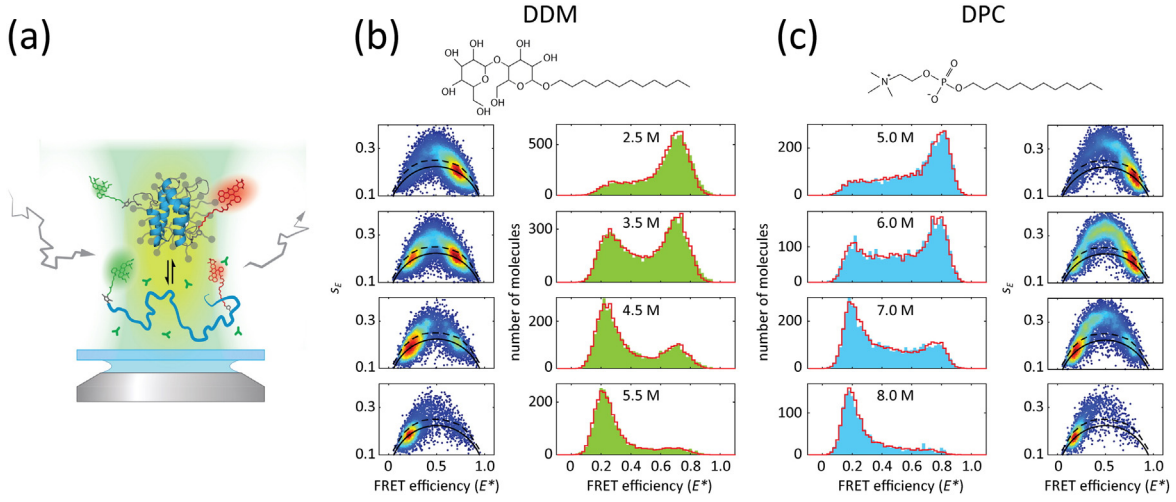

Fig. 1. (a) Single-molecule FRET confocal spectroscopy approach for investigating equilibrium (un)folding kinetics in membrane-mimetic environments. Illustration of fluorescently labeled Mistic (PDB file: 1YGM) changing its conformation between folded and unfolded states while freely diffusing through the femtoliter-sized observation volume of the confocal microscope. Increasing concentrations of urea (green forked crosses) are used to denature the protein in the presence of detergent micelles (gray). Structural changes are monitored on the basis of differences in FRET efficiency between the folded and unfolded conformations. (b, c) FRET efficiency histograms from equilibrium (un)folding experiments in the presence of micelles composed of DDM (panel b, green) or DPC (panel c, blue) at different urea concentrations (c_{urea}). Two-state dPDA fits to the histograms are shown as red cityscapes. Side panels: 2D BVA scatter plots of the burstwide FRET standard deviation (s_E) plotted against FRET efficiency (E^*). The normalized density of single molecules is color coded (scaled from blue to red). Black lines represent the standard deviation (σ_{SN}) expected for a shot-noise-limited distribution of static molecules. Dashed lines indicate the upper margin of the 99.9% confidence interval that discriminates static from dynamic molecules, with bursts above the confidence boundary exhibiting millisecond folding kinetics.

membrane-mimetic interface. Employing a chemical-denaturation approach, we study the equilibrium folding kinetics of the membrane-interacting self-inserting protein Mistic [32] (Fig. 1a) in various micellar environments as well as in aqueous buffer solution. Mistic is a 110-residue protein that assumes a simple four-helix topology and is essential for biofilm formation by *Bacillus subtilis* [33] with homologs in other Gram-positive bacteria [32,34]. Upon exposure to the denaturant urea, Mistic unfolds reversibly from various detergent micelles in a two-state manner [15], and its urea-unfolded state is largely devoid of secondary structure [35] and dissociated from micelles [36]; thus, the unfolded state can serve as a reference state that is independent of the detergent used for solubilizing the folded state [15]. Because of its unusual hydrophilic properties—Mistic contains a large number of polar and charged residues—its conformational stability depends on both hydrophobic burial within the micelle core as well as polar headgroup contacts [15], thus providing a unique opportunity for probing the effects of both polar and hydrophobic properties on protein-folding kinetics. In the following, we dissect the role of polar and hydrophobic detergent moieties and provide links between the conformational stability of a membrane-interacting protein and its folding kinetics within a hydrophilic/hydrophobic interface. We find that polar and hydrophobic detergent moieties play very different roles in shaping the folding landscape of Mistic, and together, can speed up the folding reaction to reach kinetics in the ultrafast microsecond time regime.

Results

Fast two-state folding in zwitterionic and non-ionic micelles

In a first set of experiments, we compared folding of Mistic in micelles composed of the non-ionic detergent *n*-dodecyl-β-D-maltopyranoside (DDM) with folding in the zwitterionic detergent *n*-dodecylphosphocholine (DPC). To this end, we created a protein variant ($Mistic_{30–110}$) labeled with donor (ATTO532) and acceptor (ATTO647N) fluorophores at residues 30 and 110, respectively (see Materials and Methods), and subjected the labeled protein to increasing concentrations of urea in the presence of DDM or DPC. Conformational changes were monitored by probing FRET efficiencies of individual, freely diffusing Mistic molecules using confocal single-molecule fluorescence spectroscopy. FRET efficiencies were calculated from a large number of single-molecule events and sorted into histograms.

Fig. 1b and c (center panels) depicts representative FRET efficiency histograms derived from urea-induced equilibrium (un)folding experiments in DDM and DPC. Mistic exhibited a two-state folding behavior in both detergents, as manifested in the coexistence of two FRET efficiency peaks representing the folded and unfolded states. With increasing urea concentration, the occupancy of the folded state with high FRET efficiency gradually decreased, while the low-FRET peak representing the unfolded state increased. In accordance with previous ensemble studies [15], the resilience of Mistic against chemical denaturation was higher in zwitterionic DPC than in non-ionic DDM, as reflected in a shift of the midpoint urea concentration (at which 50% of all protein molecules were folded) from ~3.5 M urea in DDM to ~6.0 M urea in DPC. Notably, the folded- and unfolded-state peaks in these histograms (Fig. 1b, c) are not well separated but connected by a pronounced bridge-like population. This population originates from dynamic interconversion, that is, from protein molecules that fold or unfold during the observation time of ~2 ms, which was corroborated by a Viterbi path reconstruction (Fig. S2) and burst-variance analysis (BVA) [37], an analytical tool that detects millisecond dynamics on the basis of the standard deviations of the FRET efficiency within a given burst (s_E). Plotting s_E *versus* FRET efficiency revealed arc-shaped distributions at intermediate FRET efficiencies (Fig. 1b, c, side panels), typical of dynamically interconverting species with interconversion rates on the millisecond timescale [29]. We further confirmed the observation of dynamics using a FRET–two-channel kernel-based density distribution estimator (FRET-2CDE) and by correlating the relative donor lifetime ($\tau_{D(A)}/\tau_{D(0)}$) with FRET efficiency (Fig. S3). When comparing histograms and BVA plots among the two series around midpoint conditions, both the inter-peak FRET efficiency and the arc-shaped BVA distributions are more populated in the presence of DPC than in DDM. This indicates more frequent interconversions between the folded and the unfolded states and, by extension, a faster (un)folding timescale (i.e., a higher relaxation rate constant k_{obs}) in DPC than in DDM.

Link between folding kinetics and equilibrium stability

After identifying two-state millisecond folding, we quantified the influence of DDM and DPC on Mistic's folding and unfolding kinetics. To this end, we used dynamic probability-distribution analysis (dPDA) [38], a method that remodels the FRET efficiency distribution to retrieve the underlying folding and unfolding rate constants (k_F and k_U, respectively) and the FRET efficiencies (E^*_F, E^*_U) of the underlying states as well as their state fractions (p_F, p_U) from the shape of the experimental FRET efficiency histogram. We extended the two-state dPDA by accounting also for the excess widths of the folded and unfolded states in addition to shot noise (see Supplementary Data). We performed dPDA at nine different urea concentrations around

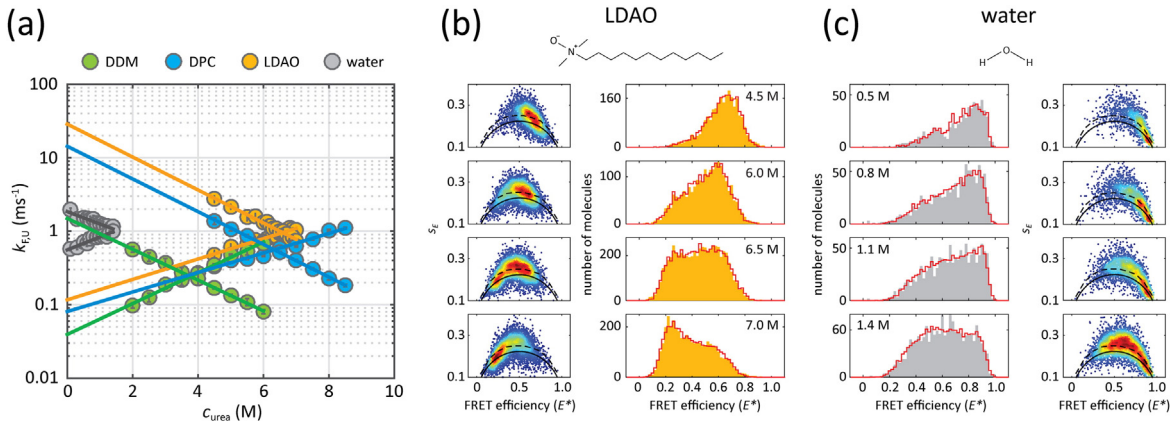

Fig. 2. (a) Kinetic analysis of Mistic$_{30–110}$ in DDM, DPC, LDAO, and water. Folding and unfolding rate constants (k_F and k_U, respectively; circles) extracted by dPDA in DDM (green), DPC (blue), LDAO (orange), or aqueous solution (gray) are plotted as functions of urea concentration (c_{urea}). Linear extrapolations are shown as solid lines. dPDA fitting error bars (gray) are smaller than symbols. (b, c) FRET efficiency histograms (center panels) from equilibrium (un)folding experiments in LDAO (panel b) or aqueous solution (panel c) at different urea concentrations. Two-state dPDA fits to histograms are shown as red cityscapes. Side panels: 2D BVA scatter plots of the burstwide FRET standard deviation (s_E) plotted against FRET efficiency (E^*).

midpoint conditions in the range between 2.5 and 5.0 M for DDM and 4.5 and 7.0 M for DPC (see Fig. S1, Supplementary Data for all histograms). Under these conditions, both the folded state and the unfolded state are significantly populated, which is essential for a reliable determination of kinetic rates using dPDA. The resulting dPDA fits yielded an excellent reconstruction of the experimentally determined FRET efficiency histograms (Fig. 1b, c, red cityscapes; extracted fit parameters are shown in Tables S1, S2 and Fig. S4, Supplementary Data). Plotting log(k_F) and log(k_U) at different urea concentrations (c_{urea}) (Fig. 2a) resulted in linear dependencies. Using linear extrapolation (see Supplementary Data), we derived $k_{F,U}^{H_2O}$, the folding and unfolding rate constants in the absence of denaturant (Fig. 2a and Table 1). We determined a folding rate constant of $k_{F,DDM}^{H_2O}$ = 1.49 ms^{-1} in the presence of DDM and, remarkably, ~10-fold faster folding with $k_{F,DPC}^{H_2O}$ = 14.3 ms^{-1} in DPC. Interestingly, the unfolding rate constants $k_{U,DDM}^{H_2O}$ = 0.039 ms^{-1} and $k_{U,DPC}^{H_2O}$ = 0.081 ms^{-1} differed only by a factor of two, indicating a weak effect of headgroup chemistry on the unfolding reaction. The substantially faster folding in DPC as compared with DDM together with similar unfolding rate constants results in a marked net stabilization of the protein in DPC over DDM, as judged from Gibbs free-energy changes in the absence of denaturant amounting to $\Delta G_{DDM}^{H_2O}$ = 9.01 kJ mol^{-1} and $\Delta G_{DPC}^{H_2O}$ = 12.8 kJ mol^{-1}. From the slopes of the folding and unfolding arms, we obtained kinetic m_F- and m_U-values, which are defined as $m_{F,U} \equiv -/+RT\partial \ln k_{F,U}/\partial c_{urea}$, with R being the universal gas constant and T the absolute temperature. We obtained $m_{F,DDM}$ = 1.20 kJ mol^{-1} M^{-1} and $m_{U,DDM}$ =1.20 kJ mol^{-1} M^{-1} in DDM and $m_{F,DPC}$ = 1.27 kJ mol^{-1} M^{-1} and $m_{U,DPC}$ = 0.76 kJ mol^{-1} M^{-1} in DPC. From the kinetic m-values, we calculated the equilibrium m-values, which are defined as $m \equiv -\partial \Delta G^{H_2O}/\partial c_{urea}$, yielding m_{DDM} = 2.40 kJ mol^{-1} M^{-1} and m_{DPC} = 2.03 kJ mol^{-1} M^{-1}.

Performing the same set of experiments on a differently labeled protein variant (Mistic$_{3–110}$) yielded, within error, identical results (see Fig. S5 and Table S7, Supplementary Data), indicating that the labeling position did not affect the obtained parameters. We further validated our approach of calculating equilibrium values from kinetic single-molecule FRET measurements by comparing it with a standard ensemble approach (see Fig. S6, Supplementary

Table 1. Kinetic and thermodynamic parameters of Mistic$_{30–110}$ (un)folding in the presence of detergent micelles or in aqueous buffer

	$k_F^{H_2O}$ (ms^{-1})	$k_U^{H_2O}$ (ms^{-1})	m_F (kJ mol^{-1}M^{-1})	m_U (kJ mol^{-1}M^{-1})	m (kJ mol^{-1}M^{-1})	ΔG^{H_2O} (kJ mol^{-1})
DDM	1.49	0.039	1.20	1.20	2.40	9.01
	(1.31–1.70)	(0.035–0.044)	(1.13–1.26)	(1.14–1.25)	(2.28–2.51)	(8.42–9.61)
DPC	14.3	0.081	1.27	0.76	2.03	12.8
	(12.6–16.3)	(0.073–0.090)	(1.22–1.32)	(0.72–0.79)	(1.95–2.11)	(12.3–13.4)
LDAO	28.7	0.12	1.28	0.79	2.07	13.7
	(23.7–34.7)	(0.091–0.15)	(1.21–1.35)	(0.70–0.89)	(1.90–2.24)	(12.6–14.7)
Aqueous buffer	1.85	0.56	0.96	1.00	1.96	2.97
	(1.75–1.96)	(0.53–0.59)	(0.81–1.11)	(0.89–1.12)	(1.69–2.23)	(2.71–3.24)

Data). Trp fluorescence equilibrium (un)folding experiments of unlabeled $Mistic_{30-110}$ in DDM yielded $\Delta G°(H_2O)$ = (9.8 ± 1.5) kJ mol^{-1} and an *m*-value of (2.4 ± 0.4) kJ mol^{-1} M^{-1}, in good agreement with the values obtained from single-molecule kinetic measurements.

Accelerated folding in a more stabilizing environment

To address the question whether faster folding in DPC is peculiar to this detergent or originates more broadly from interactions with detergents carrying zwitterionic headgroups, we performed experiments in the presence of the zwitterionic detergent lauryldimethylamine *N*-oxide (LDAO), which has been shown to confer even greater stability to Mistic [15]. Figure 2b (right panels) shows the obtained FRET efficiency histograms, where the protein was subjected to increasing concentrations of urea (see Fig. S1, Supplementary Data for all histograms). Note that experiments in the presence of LDAO were possible only up to 7 M urea, as LDAO precipitated at higher denaturant concentrations. Unfolding of Mistic occurred at elevated urea concentrations with a midpoint of ~6.5 M. Notably, and in contrast with DDM and DPC, where we observed separated folded- and unfolded-state peaks (Fig. 1b, c), the LDAO histograms showed very broad distributions with variable slopes at the high- and low-FRET efficiency flanks. This indicates even higher folding and unfolding rates, as the intermediate bridge-like FRET efficiency population increases with increasing relaxation rate. The BVA (Fig. 2b, left panels) confirmed that the broad continuous distributions observed in the LDAO histograms originate from a highly dynamic two-state equilibrium between folded and unfolded states. A comparison of histograms and BVA plots close to midpoint conditions further corroborates that the more pronounced bridging populations and arc-shaped distributions in LDAO reflect a higher frequency of interconversions and, thus, a higher relaxation rate constant compared with DPC. We extracted k_F and k_U values at 15 urea concentrations between 4.5 and 7.0 M using dPDA (Fig. 2a, orange symbols; extracted fit parameters are shown in Table S3 and Fig. S4, Supplementary Data) and extrapolated the data to zero denaturant concentration (Table 1). Mistic exhibited an extrapolated folding rate constant $k_{F,LDAO}^{H_2O}$ = 28.7 ms^{-1} in LDAO, that is, a twofold increase compared with DPC. The unfolding rate constant $k_{U,LDAO}^{H_2O}$ = 0.12 ms^{-1}, instead, remained on the same order as for DDM and DPC, which gave rise to a further net stabilization of the protein in LDAO to $\Delta G_{LDAO}^{H_2O}$ = 13.7 kJ mol^{-1}. The kinetic *m*-values ($m_{F,LDAO}$ = 1.28 kJ mol^{-1} M^{-1}, $m_{U,LDAO}$ = 0.79 kJ mol^{-1} M^{-1}) and the equilibrium *m*-values (m_{LDAO} = 2.07 kJ mol^{-1} M^{-1}) were very similar to the respective values in DPC.

Faster unfolding in aqueous buffer without membrane mimic

While headgroup chemistry modulates the folding rate of Mistic significantly, the unfolding rate is affected only slightly. This led to the question which role the mere presence of the nonpolar, hydrophobic interior of the micellar membrane-mimetic environment—or its absence—plays in shaping the folding free-energy landscape. Mistic strictly depends on a membrane mimic for long-term stability at moderate to high protein concentrations [15,39]; for short periods of time and at very low concentrations as employed in single-molecule FRET measurements, however, the protein is stable in micelle-free buffer. Thus, we performed urea-induced equilibrium (un)folding experiments in aqueous buffer at detergent concentrations ~15-fold below the critical micellar concentration (CMC) using Tween 20 at a concentration of 0.0005% (*w/v*) to passivate the measurement chamber. Figure 2c (left panels) shows FRET efficiency histograms where the protein was subjected to increasing concentrations of urea in aqueous solution (see Fig. S1, Supplementary Data for all histograms). At low urea concentrations (i.e., ≤ 0.5 M), a broad FRET efficiency distribution with a rising low-FRET peak indicated that the protein was only marginally stable in the absence of micelles. Midpoint conditions were observed at ~1.4 M urea, which is considerably lower than in any of the three detergents tested. We also observed here a clear bridge-like FRET population, reflecting millisecond interconversion dynamics as confirmed by BVA (Fig. 2c, right panels). Applying dPDA to the FRET efficiency histograms (cf. Table S4 and Fig. S4, Supplementary Data for extracted fit parameters) yielded rate constants of $k_{F,H_2O}^{H_2O}$ = 1.85 ms^{-1} and $k_{U,H_2O}^{H_2O}$ = 0.56 ms^{-1} (Fig. 2a, Table 1). Interestingly, $k_{F,H_2O}^{H_2O}$ is, within error, identical to that observed in DDM, while $k_{U,H_2O}^{H_2O}$ is one order of magnitude higher than in any detergent used in this study. The decreased equilibrium stability of Mistic in water ($\Delta G_{H_2O}^{H_2O}$ = 2.97 kJ mol^{-1}) thus correlates with much faster unfolding as compared with DDM, DPC, and LDAO. The *m*-values amounted to m_{F,H_2O} = 0.96 kJ mol^{-1} M^{-1}, m_{U,H_2O} = 1.00 kJ mol^{-1} M^{-1}, and m_{H_2O} = 1.96 kJ mol^{-1} M^{-1}, which is slightly lower than the values in DPC and LDAO.

Discussion

Ultrafast protein folding at a hydrophobic/hydrophilic interface

Urea-induced equilibrium (un)folding experiments in the presence of detergent micelles and aqueous buffer reveal that Mistic is a fast two-state folding protein

(Figs. 1 and 2, Table 1), with folding and unfolding rate constants in the millisecond time regime. The folding kinetics of Mistic is strongly modulated by the choice of detergent, leading up to a ~20-fold increase in the presence of zwitterionic detergents as compared with non-ionic ones. In particular, DPC and LDAO accelerate folding to $\tau_{F,DPC}^{H_2O}$ = 70 μs and $\tau_{F,LDAO}^{H_2O}$ = 35 μs, respectively. Thus, we have identified a protein for which ultrafast folding can be induced by a hydrophobic/hydrophilic interface between a hydrocarbon phase and zwitterionic headgroups, both of which lead to a significant speed-up of the folding reaction. Given the similar topology of the protein in all detergents [15], this illustrates the strong influence of the environment on the folding free-energy landscape. Although protein size and topology have been identified as key players in determining the folding speed of soluble proteins [4–8], there is room for modulation by environmental factors. A topological analysis based on the contact order predicts folding rates between 10 μs [8] and 8 ms [40] for Mistic, which agrees well with the range of our experimentally determined folding times. While the rates calculated for vanishing denaturant concentrations involve rather long extrapolations based on a linear dependence on denaturant concentration, the measured folding rates at midpoint conditions are close to the Finkelstein speed limit of $k_F^{midpoint} \approx 1\ ms^{-1}$ calculated for a 110-residue protein [1]. Particularly, folding in DPC and LDAO at the midpoint occurs with $k_{F,DPC}^{midpoint} \approx 0.55\ ms^{-1}$ and $k_{F,LDAO}^{midpoint} \approx 1.0\ ms^{-1}$, respectively, thus supporting the observation of ultrafast folding under "extrapolated" conditions of zero denaturant. Interestingly, previous NMR experiments on Mistic unfolding in the presence of LDAO have reported a gradual loss of secondary structure but not all tertiary structure with increasing denaturant concentration [35]. By contrast, our single-molecule FRET data clearly follow a two-state folding behavior even in LDAO. In reconciling these observations, it is important to consider the different temporal resolutions of the two methods: while, on this timescale, NMR experiments provide time-averaged structures, single-molecule FRET allows access to folding-state lifetimes in the microsecond time range.

Modulation of protein-folding landscapes by hydrophobic and polar detergent moieties

Hydrophobic and polar detergent moieties exert opposing effects on the folding and unfolding rates of Mistic: Hydrophobicity plays a major role in modulating the unfolding path, as the protein unfolds approximately 10 times slower in a membrane mimic than in aqueous buffer. The small variations in the unfolding kinetics among the three detergents indicate that the unfolding process is little affected by headgroup chemistry and, thus, primarily governed by the hydrophobic micelle core. Conversely, interactions with detergents carrying zwitterionic headgroups are the prime determinants in accelerating the folding reaction up to ~20-fold. Consequently, with reference to an aqueous environment, hydrophobic burial in the hydrocarbon core of detergent micelles strongly stabilizes the folded state, and zwitterionic headgroups contribute further to stability as compared with neutral ones (Table 1). Figure 3 summarizes these conclusions, which are based on the earlier finding that the unfolded state is independent of the detergent used to solubilize the native state and therefore may serve as a common reference state in all environments [15,35,36]. Using the kinetic rates, we estimated the free-energy barriers associated with folding by assuming that the speed limit [2] of $\tau_{F,min} = (N/100)$ μs = 1.1 μs, with N = 110 denoting the number of amino acid residues, corresponds to the pre-exponential factor τ_0. The folding free-energy barrier can then be calculated as $\Delta G_F^{\#} = RT\ln(\tau_F/\tau_0)$, yielding $\Delta G_{F,LDAO}^{\#} = 8.6\ kJ\ mol^{-1}$ and $\Delta G_{F,DPC}^{\#} = 10.3\ kJ\ mol^{-1}$, whereas the barriers in DDM and water are $\Delta G_{F,DDM}^{\#} = 15.9\ kJ\ mol^{-1}$ and $\Delta G_{F,H_2O}^{\#} = 15.4\ kJ\ mol^{-1}$. Although these estimates rely on approximations, they suggest that the folding barriers in zwitterionic detergent micelles are very small and close to the 3 RT (~7.4 kJ mol^{-1}) limit of barrierless folding at room temperature [41].

Interactions with micelles obviously affect the exposure of Mistic to the aqueous solvent, as reflected in the equilibrium as well as the kinetic m-values (Table 1). Equilibrium m-values have been shown to be a measure of the change in solvent-accessible surface between the folded and unfolded states [15,42]. Since the unfolded state is a common reference state in all environments, the effects on the m-values in different environments reflect differences in the solvent-accessible area of the folded state. The larger value in DDM compared with that in aqueous buffer indicates that Mistic's folded state is more effectively shielded from the solvent and buried inside the core of non-ionic DDM micelles than in aqueous solution. Conversely, in DPC and LDAO, the equilibrium m-values are, within error, the same as in

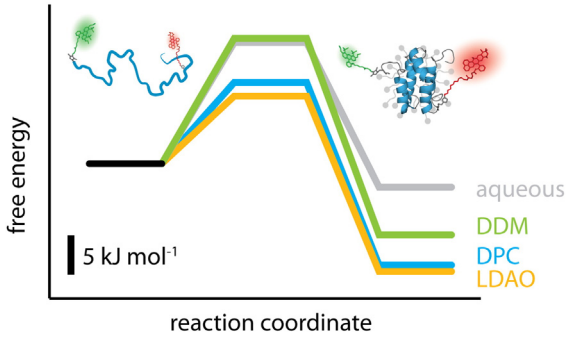

Fig. 3. One-dimensional free-energy profiles of Mistic$_{30–110}$ folding in DDM, DPC, and LDAO micelles as well as in aqueous solution.

aqueous buffer, which can be explained by more extensive hydration and deeper water penetration into the headgroup region of zwitterionic micelles. Similarly, kinetic *m*-values are related to the degree of change in the average solvent-accessible surface area between, on the one hand, the transition state and, on the other hand, the unfolded or folded state, respectively. For folding into micelles, the m_F-values in all three detergents are similar but significantly larger compared with folding in water. Taking the unfolded state as a common reference state, this is readily explained by increased shielding of protein surface in the transition state within micelles, whereas in the absence of a membrane mimic, the transition state remains exposed to the aqueous solvent. In the unfolding reaction, the low kinetic *m*-values in DPC and LDAO reflect a smaller change in solvent-accessible area of the transition state as compared with DDM, while water takes an intermediate position. Furthermore, the ratio of the kinetic *m*-value to the equilibrium *m*-value, also known as the Tanford β-value ($\beta_F \equiv m_F/m$), provides a measure of the relative solvent accessibility of the transition state and, thus, the compactness of the transition state relative to the native state. We obtain $\beta_{F,aqueous} = 0.49$, $\beta_{F,DDM} = 0.50$, $\beta_{F,DPC} = 0.63$, and $\beta_{F,LDAO} = 0.62$, suggesting that the transition state is relatively more compact in zwitterionic micelles than in aqueous buffer or non-ionic micelles.

Further information on the transition state, in particular on the formation of stabilizing interactions along the reaction coordinate, can be obtained from correlations of the equilibrium stability and the folding barrier. By analogy to the so-called φ-value [43] used in mutational protein-folding studies, we define a "solvent" φ_{sol}-value as $\varphi_{sol} \equiv \Delta\Delta G_F^{\#}/\Delta\Delta G^{H_2O}$, which relates the change in protein stability, $\Delta\Delta G^{H_2O}$, to the change in the height of the free-energy barrier, $\Delta\Delta G_F^{\#}$. Here, the first Δ refers to the difference in stability between one of the micellar membrane mimics and aqueous buffer. Therefore, this parameter provides a measure of the extent to which an equilibrium-stability change caused by the environment is reflected in the transition state and reports on the influence of the environment on the formation of stabilizing interactions in the transition state: A membrane mimic that stabilizes—that is, lowers the free energy of—the transition state speeds up folding; by contrast, an environment in which only the equilibrium stability is enhanced without lowering the transition-state barrier to folding has no effect on the kinetics of folding. We obtained $\varphi_{sol,DDM} = -0.09$, $\varphi_{sol,DPC} = 0.51$, and $\varphi_{sol,LDAO} = 0.64$. Accordingly, DDM has a negligible influence on the transition state and stabilizes the folded state only, whereas the higher values in DPC and LDAO indicate that, in addition to stabilizing the folded state, the transition state is stabilized in the presence of zwitterionic detergents. In summary, while hydrophobic burial stabilizes only the folded state but not the transition state, polar headgroup interactions stabilize the folded state and, additionally, lower the free-energy barrier to speed up the folding reaction.

Role of polar interactions and micelle properties in speeding up protein folding

The substantially higher folding rate constants of Mistic in DPC and LDAO as compared with DDM and aqueous buffer suggest a role for polar interactions in enabling ultrafast folding. Electrostatic focusing has been demonstrated to accelerate the binding of ligands to proteins [44,45] as well as the coupled binding and folding of intrinsically disordered proteins [46]. Similarly, Coulombic effects could be at play when Mistic, which contains a total of 25 acidic and 15 basic amino acid residues, associates with and folds into zwitterionic micelles. Such effects may not only enhance the encounter rate by efficiently targeting the protein to the micelle but also increase the dwell time at the micelle and reduce the detachment rate after encounter to increase the probability of folding at the micelle surface. Furthermore, zwitterionic detergent micelles [47] and phospholipid bilayers [48] possess a pronounced positive interfacial dipole potential of up to a few hundred millivolts inside their nonpolar core, which is absent from nonionic detergent micelles. The positive membrane dipole potential has been suggested as a driving force for the coupled folding and bilayer insertion of an anionic β-barrel membrane protein [49]. As Mistic has a net negative charge of −13 at pH 7.4, the positive dipole potential might help in reducing the free-energy costs associated with crossing the activation barrier and accommodating the rather hydrophilic protein in the micelle during folding. Furthermore, also the higher φ_{sol}-values in DPC and LDAO pinpoint toward a lowering of the folding barrier in zwitterionic micelles caused by favorable contacts of the transition state with the micelle. This is supported by observations from NMR experiments in which the assembly of the four-helix bundle in the presence of LDAO starts from helices 3 and 4 and then proceeds through recruitment of helix 2 and finally helix 1 [35]. This study also found that helix 3 as well as loop 2 and helix 4 retain close contacts with LDAO headgroups even at high denaturant concentrations, indicating that these regions, which comprise the folding core, interact with the zwitterionic micellar surface even in the unfolded state. Since the folding core of Mistic possesses a high negative charge density with anionic groups on the protein surface mainly clustered around the third helical segment of the folded protein [15] and anions have a high affinity for zwitterionic micellar surfaces because of their positive interfacial dipole potential, the local negative charge density facilitates orientation of Mistic's folding core at the zwitterionic micellar

surface and, through Coulombic priming, assists in establishing polar contacts with the zwitterionic headgroups early during the folding process.

While polar interactions might influence the folding speed directly, the acceleration observed in the presence of zwitterionic micelles might also stem from differences in surface properties that impact the accessibility of the micelle interior to the protein. In DDM micelles, the polar but uncharged maltose headgroups are densely packed because of inter- and intra-headgroup hydrogen bonding, thus yielding an average occupied surface area per monomer of only 60–70 $Å^2$ despite the relatively large steric size of the headgroup [50,51]. This results in hydration numbers as low as 3–5 water molecules per glucose subunit of the maltose headgroup and largely precludes water penetration into the micellar interface, with essentially no water molecules within ~17 Å of the micelle center of mass (COM) [50]. By contrast, DPC monomers experience electrostatic repulsion between their zwitterionic headgroups, thereby resulting in a larger average surface area of ~78 $Å^2$ per monomer despite the comparably small steric size of the phosphocholine headgroup. This allows more extensive penetration of water molecules, as reflected in hydration numbers of ~21 and ~8 for the choline and phosphate moieties, respectively [52], and substantial penetration of water even within ~12 Å of the COM [52,53]. LDAO micelles feature an even larger surface area of ~95 $Å^2$ per monomer, a hydration number of ~8 per headgroup, and deep penetration of water molecules within 10–12 Å of the COM [54,55]. Thus, the higher folding rate constants of Mistic in DPC and LDAO as compared with DDM are also correlated with the less densely packed, more hydrated interfacial regions of zwitterionic micelles. These properties might further help reduce the free-energy costs associated with crossing the activation barrier as well as accommodating and hydrating the polar protein within the micelle upon folding.

In addition, zwitterionic micelle surfaces have been shown to cause partial neutralization of Glu and Asp residues in proteins [18,56] by shifting the ionization equilibrium of the carboxylate groups toward the non-ionized species [18] and increasing the local proton concentration (i.e., pH drop) as a result of the negative surface potential [57]. Such charge-neutralization effects have been implicated in determining the folding kinetics of membrane proteins [18]. Therefore, the partially neutralized anionic character of Mistic in the vicinity of a zwitterionic micelle surface may further serve to lower the barrier for coupled binding and folding into the hydrophobic micelle core.

Biological implication of fast folding modulation at a hydrophobic/hydrophilic interface

Our results show that zwitterionic headgroup moieties at a hydrophobic/hydrophilic interface can tailor the folding landscape of Mistic to achieve ultrafast kinetics with marginal folding barriers. An important question that emerges from these findings is why this protein is subject to such kinetic regulation. Fast conformational transitions between folded and unfolded states at micellar surfaces resemble the fast coupled folding and binding of intrinsically disordered proteins with their interaction partners [58], which has been shown to aid in either induced-fit or conformational-selection mechanisms to facilitate moonlighting [59] or produce sophisticated allosteric effects in proteins that bind to multiple, structurally diverse partners [60]. Fast conformational motions also ensure conformational selection by a quick locking and homing-to-target mechanism [58]. Moreover, it has been suggested that fast-folding proteins with marginal barriers may confer an advantage in signaling by acting as a continuous regulator [58,61,62]. Interestingly, Mistic is essential for biofilm formation and is part of an auto-regulatory feedback loop involving K^+ efflux and activation of kinases and biofilm regulatory factors in a complex signaling pathway [33]. Although folding at membranes is clearly different from folding into micelles, it is tempting to speculate that similar mechanisms could be at play for fine-tuning interactions with the bacterial membrane, which is rich in zwitterionic headgroups, or with potential protein interaction partners at the membrane such as the K^+ channel YugO [33].

Conclusions

Protein folding is a complex physicochemical self-organization process dictated by an interplay of forces determined by both the sequence of the protein itself and the properties of the environment. The dependence of the folding reaction on the environment adds complexity that can have a strong impact not only on the structure of the folded state but also on its dynamic equilibrium with the unfolded state. This applies to all proteins that depend on interactions with other biomolecules for proper folding but is particularly relevant for self-inserting membrane-interacting proteins. Using single-molecule spectroscopy to extract folding kinetics in micellar environments under equilibrium conditions, we have shown that polar and nonpolar moieties play differential roles in shaping the folding landscape of a membrane-interacting protein. Hydrophobic burial mainly stabilizes the protein against unfolding, while zwitterionic headgroups, abundant also in biological membranes, significantly lower the folding barrier. Together, these effects give rise to ultrafast folding in a heterogeneous, anisotropic environment, shedding light on novel kinetic control mechanisms of protein-folding reactions by physicochemical properties of a hydrophobic/hydrophilic interface.

Materials and Methods

Preparation of labeled protein

A protein variant ($Mistic_{30–110}$) for site-specific double-labeling was engineered with an unnatural amino acid (*N*-propargyl-L-lysine, PrK, SiChem, Germany) and a unique Cys incorporated at residues 30 and 110, respectively [29]. Recombinant protein production was performed in *Escherichia coli* using the pEvol vector system (pEvol PylRS) from *Methanosarcina mazei* for incorporation of PrK [63]. After purification following published procedures [15,35], the protein was orthogonally labeled at residue 30 with acceptor (ATTO647N, Atto-Tec, Germany) and at residue 110 with donor (ATTO532, Atto-Tec) fluorophores using alkyne–azide click chemistry and thiol–maleimide coupling [64]. Details are given in the Supplementary Data.

Single-molecule FRET measurements

Experiments were carried out using a custom-built dual-color single-molecule confocal fluorescence microscope [65,66]. Details on instrumentation are given in the Supplementary Data. Measurements were performed at 24 °C in 50 mM Tris buffer (pH 7.4), 50 mM NaCl with various concentrations of urea (Ultrapure, Carl Roth, Germany) containing detergent micelles composed of either DDM (Anatrace, USA), DPC (Anatrace, USA), or LDAO (Sigma, USA). The detergent concentration was always 1 mM above its CMC at the respective urea concentration as determined elsewhere [15,24]. Urea and detergents were of highest purity grade commercially available. Experiments in aqueous solution were performed in buffer containing 0.0005% (*w*/*v*) Tween 20 (Sigma, USA), ~15 times below the CMC, to prevent surface adhesion. The labeled protein was examined at ~5 pM in its respective aqueous or micellar environment to obtain appropriate burst rates under single-molecule conditions.

Data analysis

Data analysis was performed with custom-written Matlab scripts (Mathworks, USA). The analysis software is available upon request. Single-molecule events were identified from the acquired photon stream by a burst search algorithm. FRET efficiency histograms were obtained after removal of donor-only, acceptor-only, and blinking and photobleaching events. Details are given in the Supplementary Data. Identification of millisecond folding kinetics was done by BVA [37] as described in the Supplementary Data. Quantification of millisecond folding and unfolding rates from FRET efficiency histograms was performed by dPDA [38] as detailed in the Supplementary Data. Kinetic and thermodynamic parameters were derived by applying linear extrapolation to extract folding and unfolding rates in the absence of denaturant as outlined in the Supplementary Data.

Acknowledgments

We are very grateful to Prof. Tobin Sosnick (University of Chicago, USA) for stimulating discussions and comments on the manuscript. We also thank all members of the Schlierf and Keller groups for discussions. The pEvol PylRS plasmid was kindly provided by Dr. Edward A. Lemke (EMBL, Heidelberg, Germany). This work was supported by the German Federal Ministry of Education and Research BMBF with grant 03Z2EN11 to M.S., the Deutsche Forschungsgemeinschaft with grants KE 1478/4-1 to S.K. and SCHL 1896/3-1 to M.S., and the Stipendienstiftung Rheinland-Pfalz with a scholarship to G.K.

Appendix A. Supplementary data

Supplementary Data accompanying this manuscript: Details on protein preparation, single-molecule FRET confocal spectroscopy, and data analysis including BVA and dPDA as well as calculation of kinetic and thermodynamic parameters; entire series of FRET efficiency histograms; extracted dPDA parameters in tabular form; Viterbi path reconstruction at midpoint conditions; extended dynamics analysis at different denaturant conditions; dependence of FRET efficiencies of folded and unfolded states on denaturant concentration; additional single-molecule FRET data from a different labeling variant and ensemble equilibrium (un)folding of unlabeled protein. Supplementary data associated with this article can be found in the online version at https://doi.org/10.1016/j.jmb.2017.10.031.

Received 9 August 2017;
Received in revised form 12 October 2017;
Accepted 27 October 2017
Available online 8 November 2017

Keywords:
ultrafast folding;
folding kinetics;
single-molecule FRET;
Mistic;
membrane protein

The authors declare no conflict of interest.

Abbreviations used:
DDM, *n*-dodecyl-β-D-maltopyranoside; DPC, *n*-dodecylphosphocholine; LDAO, lauryldimethylamine *N*-oxide; FRET, Förster resonance energy transfer; dPDA, dynamic probability-distribution analysis; BVA, burst-variance analysis; COM, center of mass; CMC, critical micellar concentration.

References

[1] S.O. Garbuzynskiy, D.N. Ivankov, N.S. Bogatyreva, A.V. Finkelstein, Golden triangle for folding rates of globular proteins, Proc. Natl. Acad. Sci. U. S. A. 110 (2013) 147–150.
[2] J. Kubelka, J. Hofrichter, W.A. Eaton, The protein folding "speed limit", Curr. Opin. Struct. Biol. 14 (2004) 76–88.
[3] T.R. Sosnick, D. Barrick, The folding of single domain proteins—have we reached a consensus? Curr. Opin. Struct. Biol. 21 (2011) 12–24.
[4] G.C. Rollins, K.A. Dill, General mechanism of two-state protein folding kinetics, J. Am. Chem. Soc. 136 (2014) 11420–11427.
[5] A.N. Naganathan, V. Muñoz, Scaling of folding times with protein size, J. Am. Chem. Soc. 127 (2005) 480–481.
[6] K.W. Plaxco, C. Spitzfaden, I.D. Campbell, C.M. Dobson, A comparison of the folding kinetics and thermodynamics of two homologous fibronectin type III modules, J. Mol. Biol. 270 (1997) 763–770.
[7] K.W. Plaxco, K.T. Simons, I. Ruczinski, D. Baker, Topology, stability, sequence, and length: defining the determinants of two-state protein folding kinetics, Biochemistry 39 (2000) 11177–11183.
[8] K.W. Plaxco, K.T. Simons, D. Baker, Contact order, transition state placement and the refolding rates of single domain proteins, J. Mol. Biol. 277 (1998) 985–994.
[9] M. Gruebele, K. Dave, S. Sukenik, Globular protein folding in vitro and in vivo, Annu. Rev. Biophys. 45 (2016) 233–251.
[10] A. Dhar, A. Samiotakis, S. Ebbinghaus, L. Nienhaus, D. Homouz, M. Gruebele, M.S. Cheung, Structure, function, and folding of phosphoglycerate kinase are strongly perturbed by macromolecular crowding, Proc. Natl. Acad. Sci. U. S. A. 107 (2010) 17586–17591.
[11] J. Mittal, R.B. Best, Thermodynamics and kinetics of protein folding under confinement, Proc. Natl. Acad. Sci. U. S. A. 105 (2008) 20233–20238.
[12] B. van den Berg, R. Wain, C.M. Dobson, R.J. Ellis, Macromolecular crowding perturbs protein refolding kinetics: implications for folding inside the cell, EMBO J. 19 (2000) 3870–3875.
[13] A. Rath, C.M. Deber, Protein structure in membrane domains, Annu. Rev. Biophys. 41 (2012) 135–155.
[14] S. Fiedler, J. Broecker, S. Keller, Protein folding in membranes, Cell. Mol. Life Sci. 67 (2010) 1779–1798.
[15] J. Broecker, S. Fiedler, K. Gimpl, S. Keller, Polar interactions trump hydrophobicity in stabilizing the self-inserting membrane protein Mistic, J. Am. Chem. Soc. 136 (2014) 13761–13768.
[16] D. Gessmann, Y.H. Chung, E.J. Danoff, A.M. Plummer, C.W. Sandlin, N.R. Zaccai, K.G. Fleming, Outer membrane β-barrel protein folding is physically controlled by periplasmic lipid head groups and BamA, Proc. Natl. Acad. Sci. U. S. A. 111 (2014) 5878–5883.
[17] H. Hong, L.K. Tamm, Elastic coupling of integral membrane protein stability to lipid bilayer forces, Proc. Natl. Acad. Sci. U. S. A. 101 (2004) 4065–4070.
[18] D.E. Otzen, Protein unfolding in detergents: effect of micelle structure, ionic strength, pH, and temperature, Biophys. J. 83 (2002) 2219–2230.
[19] K.G. Fleming, Energetics of membrane protein folding, Annu. Rev. Biophys. 43 (2014) 233–255.
[20] N.J. Harris, P.J. Booth, Folding and stability of membrane transport proteins in vitro, Biochim. Biophys. Acta 1818 (2012) 1055–1066.
[21] J.U. Bowie, Solving the membrane protein folding problem, Nature 438 (2005) 581–589.
[22] D.E. Otzen, K.K. Andersen, Folding of outer membrane proteins, Arch. Biochem. Biophys. 531 (2013) 34–43.
[23] S.H. White, W.C. Wimley, Membrane protein folding and stability: physical principles, Annu. Rev. Biophys. Biomol. Struct. 28 (1999) 319–365.
[24] J. Broecker, S. Keller, Impact of urea on detergent micelle properties, Langmuir 29 (2013) 8502–8510.
[25] R.E. Burton, G.S. Huang, M.A. Daugherty, T.L. Calderone, T.G. Oas, The energy landscape of a fast-folding protein mapped by Ala → Gly substitutions, Nat. Struct. Biol. 4 (1997) 305–310.
[26] V. Muñoz, J.M. Sanchez-Ruiz, Exploring protein-folding ensembles: a variable-barrier model for the analysis of equilibrium unfolding experiments, Proc. Natl. Acad. Sci. U. S. A. 101 (2004) 17646–17651.
[27] P.R. Banerjee, A.A. Deniz, Shedding light on protein folding landscapes by single-molecule fluorescence, Chem. Soc. Rev. 43 (2014) 1172–1188.
[28] B. Schuler, H. Hofmann, Single-molecule spectroscopy of protein folding dynamics—expanding scope and timescales, Curr. Opin. Struct. Biol. 23 (2013) 36–47.
[29] A. Hartmann, G. Krainer, S. Keller, M. Schlierf, Quantification of millisecond protein-folding dynamics in membrane-mimetic environments by single-molecule Förster resonance energy transfer spectroscopy, Anal. Chem. 87 (2015) 11224–11232.
[30] G. Krainer, P. Gracia, E. Frotscher, A. Hartmann, P. Gröger, S. Keller, M. Schlierf, Slow interconversion in a heterogeneous unfolded-state ensemble of outer-membrane phospholipase A, Biophys. J. 113 (2017) 1280–1289.
[31] R.E. Jefferson, D. Min, K. Corin, J.Y. Wang, J.U. Bowie, Applications of single-molecule methods to membrane protein folding studies, J. Mol. Biol. (2017) https://doi.org/10.1016/j.jmb.2017.05.021.
[32] T.P. Roosild, J. Greenwald, M. Vega, S. Castronovo, R. Riek, S. Choe, NMR structure of Mistic, a membrane-integrating protein for membrane protein expression, Science 307 (2005) 1317–1321.
[33] M.E. Lundberg, E.C. Becker, S. Choe, MstX and a putative potassium channel facilitate biofilm formation in *Bacillus subtilis*, PLoS One 8 (2013), e60993.
[34] J. Marino, N. Bordag, S. Keller, O. Zerbe, Mistic's membrane association and its assistance in overexpression of a human GPCR are independent processes, Protein Sci. 24 (2015) 38–48.
[35] T. Jacso, B. Bardiaux, J. Broecker, S. Fiedler, T. Baerwinkel, A. Mainz, U. Fink, C. Vargas, H. Oschkinat, S. Keller, B. Reif, The mechanism of denaturation and the unfolded state of the α-helical membrane-associated protein Mistic, J. Am. Chem. Soc. 135 (2013) 18884–18891.
[36] K. Gimpl, J. Klement, S. Keller, Characterising protein/detergent complexes by triple-detection size-exclusion chromatography, Biol. Proced. Online 18 (2016) 4.

[37] J.P. Torella, S.J. Holden, Y. Santoso, J. Hohlbein, A.N. Kapanidis, Identifying molecular dynamics in single-molecule FRET experiments with burst variance analysis, Biophys. J. 100 (2011) 1568–1577.
[38] Y. Santoso, J.P. Torella, A.N. Kapanidis, Characterizing single-molecule FRET dynamics with probability distribution analysis, ChemPhysChem 11 (2010) 2209–2219.
[39] H. Dvir, M.E. Lundberg, S.K. Maji, R. Riek, S. Choe, Mistic: cellular localization, solution behavior, polymerization, and fibril formation, Protein Sci. 18 (2009) 1564–1570.
[40] E. Capriotti, R. Casadio, K-fold: a tool for the prediction of the protein folding kinetic order and rate, Bioinformatics 23 (2007) 385–386.
[41] F. Liu, M. Gruebele, Downhill dynamics and the molecular rate of protein folding, Chem. Phys. Lett. 461 (2008) 1–8.
[42] J.K. Myers, C. Nick Pace, J. Martin Scholtz, Denaturant *m* values and heat capacity changes: relation to changes in accessible surface areas of protein unfolding, Protein Sci. 4 (1995) 2138–2148.
[43] A. Matouschek, J.T. Kellis, L. Serrano, A.R. Fersht, Mapping the transition state and pathway of protein folding by protein engineering, Nature 340 (1989) 122–126.
[44] G. Schreiber, A.R. Fersht, Rapid, electrostatically assisted association of proteins, Nat. Struct. Biol. 3 (1996) 427–431.
[45] B. Honig, A. Nicholls, Classical electrostatics in biology and chemistry, Science 268 (1995) 1144–1149.
[46] D. Ganguly, W. Zhang, J. Chen, Electrostatically accelerated encounter and folding for facile recognition of intrinsically disordered proteins, PLoS Comput. Biol. 9 (2013), e1003363
[47] P. Sarkar, A. Chattopadhyay, Dipolar rearrangement during micellization explored using a potential-sensitive fluorescent probe, Chem. Phys. Lipids 191 (2015) 91–95.
[48] B.H. Honig, W.L. Hubbell, R.F. Flewelling, Electrostatic interactions in membranes and proteins, Annu. Rev. Biophys. Biophys. Chem. 15 (1986) 163–193.
[49] A.H. Dewald, J.C. Hodges, L. Columbus, Physical determinants of β-barrel membrane protein folding in lipid vesicles, Biophys. J. 100 (2011) 2131–2140.
[50] S. Abel, F.-Y. Dupradeau, E.P. Raman, A.D. MacKerell, M. Marchi, Molecular simulations of dodecyl-β-maltoside micelles in water: influence of the headgroup conformation and force field parameters, J. Phys. Chem. B 115 (2011) 487–499.
[51] R.C. Oliver, J. Lipfert, D.A. Fox, R.H. Lo, S. Doniach, L. Columbus, Dependence of micelle size and shape on detergent alkyl chain length and head group, PLoS One 8 (2013), e62488
[52] T. Wymore, X.F. Gao, T.C. Wong, Molecular dynamics simulation of the structure and dynamics of a dodecylphosphocholine micelle in aqueous solution, J. Mol. Struct. 485–486 (1999) 195–210.
[53] D.P. Tieleman, D. van der Spoel, H.J.C. Berendsen, Molecular dynamics simulations of dodecylphosphocholine micelles at three different aggregate sizes: micellar structure and chain relaxation, J. Phys. Chem. B 104 (2000) 6380–6388.
[54] C.D. Lorenz, C.M. Hsieh, C.A. Dreiss, M.J. Lawrence, Molecular dynamics simulations of the interfacial and structural properties of dimethyldodecylamine-*N*-oxide micelles, Langmuir 27 (2011) 546–553.
[55] F. Sterpone, G. Marchetti, C. Pierleoni, M. Marchi, Molecular modeling and simulation of water near model micelles: diffusion, rotational relaxation and structure at the hydration interface, J. Phys. Chem. B 110 (2006) 11504–11510.
[56] G. Wang, W.D. Treleaven, R.J. Cushley, Conformation of human serum apolipoprotein A-I(166–185) in the presence of sodium dodecyl sulfate or dodecylphosphocholine by ^{1}H-NMR and CD. Evidence for specific peptide-SDS interactions, Biochim. Biophys. Acta 1301 (1996) 174–184.
[57] J.P. Priebe, B.S. Souza, G.A. Micke, A.C.O. Costa, H.D. Fiedler, C.A. Bunton, F. Nome, Anion-specific binding to *n*-hexadecyl phosphorylcholine micelles, Langmuir 26 (2010) 1008–1012.
[58] V. Muñoz, M. Cerminara, When fast is better: protein folding fundamentals and mechanisms from ultrafast approaches, Biochem. J. 473 (2016) 2545–2559.
[59] C.J. Jeffery, Moonlighting proteins: old proteins learning new tricks, Trends Genet. 19 (2003) 415–417.
[60] A.C.M. Ferreon, J.C. Ferreon, P.E. Wright, A.A. Deniz, Modulation of allostery by protein intrinsic disorder, Nature 498 (2013) 390–394.
[61] H. Gelman, M. Gruebele, Fast protein folding kinetics, Q. Rev. Biophys. 47 (2014) 95–142.
[62] M. Cerminara, T.M. Desai, M. Sadqi, V. Muñoz, Downhill protein folding modules as scaffolds for broad-range ultrafast biosensors, J. Am. Chem. Soc. 134 (2012) 8010–8013.
[63] S. Milles, S. Tyagi, N. Banterle, C. Koehler, V. VanDelinder, T. Plass, A.P. Neal, E.A. Lemke, Click strategies for single-molecule protein fluorescence, J. Am. Chem. Soc. 134 (2012) 5187–5195.
[64] S. Tyagi, E.A. Lemke, Genetically encoded click chemistry for single-molecule FRET of proteins, Methods Cell Biol. 113 (2013) 169–187.
[65] G. Krainer, A. Hartmann, M. Schlierf, farFRET: extending the range in single-molecule FRET experiments beyond 10 nm, Nano Lett. 15 (2015) 5826–5829.
[66] A. Hartmann, G. Krainer, M. Schlierf, Different fluorophore labeling strategies and designs affect millisecond kinetics of DNA hairpins, Molecules 19 (2014) 13735–13754.